A Lactate-related LncRNA Model for Predicting Prognosis, Immune Landscape and Therapeutic Response in Breast Cancer

Jia Li
The Second Affiliated Hospital of Xi'an Jiaotong University
Fei Wu
The Second Affiliated Hospital of Xi'an Jiaotong University
Yinbin Zhang
The Second Affiliated Hospital of Xi'an Jiaotong University
Chaofan Li
The Second Affiliated Hospital of Xi'an Jiaotong University
Huizi Wu
The Second Affiliated Hospital of Xi'an Jiaotong University
Cong Feng
The Second Affiliated Hospital of Xi'an Jiaotong University
Weiwei Wang
The Second Affiliated Hospital of Xi'an Jiaotong University
Xuan Liu
The Second Affiliated Hospital of Xi'an Jiaotong University
Yu Zhang
The Second Affiliated Hospital of Xi'an Jiaotong University
Yifan Cai
The Second Affiliated Hospital of Xi'an Jiaotong University
Yiwei Jai
The Second Affiliated Hospital of Xi'an Jiaotong University
Hao Qiao
The Second Affiliated Hospital of Xi'an Jiaotong University
Shuqun Zhang (✉ shuqun_zhang1971@163.com)
The Second Affiliated Hospital of Xi'an Jiaotong University

Research Article

Keywords: lactate, long non-coding RNA, breast cancer, prognostic signature, tumor immune microenvironment, drug sensitivity.

Posted Date: May 25th, 2022

DOI: https://doi.org/10.21203/rs.3.rs-1675018/v1

Abstract

Background: Breast cancer (BC) has the highest incidence rate of all cancers globally, with high heterogeneity. Increasing evidence shows that lactate and long non-coding RNA (lncRNA) play a critical role in the occurrence, maintenance, therapeutic response, and the immune microenvironment of tumors. We aimed to construct a lactate-related lncRNAs prognostic signature (LRLPS) for BC patients to predict prognosis, tumor microenvironment, and treatment responses.

Methods: The BC data was download from the Cancer Genome Atlas (TCGA) database. The lactate-related genes were got from the Molecular Signatures Database. Difference analysis and Pearson correlation analysis were used to identify the differentially expressed lactate-related lncRNAs (LRLs). The univariate Cox regression analysis, least absolute shrinkage and selection operator (LASSO), and multivariate Cox regression analysis were used to construct the LRLPS. We performed the Kaplan–Meier survival analysis, time-dependent receiver operating characteristic (ROC) curves, and univariate and multivariate analyses to valid the LRLPS. The GO/KEGG, GSEA, CIBERSORT, ESTIMATE, Tumor Immune Dysfunction and Exclusion (TIDE), and Immunophenoscore (IPS), pRRophetic and CellMiner databases were used to explore the different tumor immune microenvironment, and treatment responses.

Results: We totally acquired 196 differentially expressed LRLs between breast tumor and normal tissues. We constructed the LRLPS with 7 LRLs. Patients could be assigned into high-risk and low-risk groups based on the medium-risk sore in the training cohort. And it was proved that the prognosis prediction ability of the LRLPS was excellent, robust, and independent. Furthermore, a nomogram was constructed based on the LRLPS risk score and clinical factors to predict the 3-, 5-, and 10-year survival probability. The two risk groups had different immune activity. The low-risk patients had higher levels of immune infiltration and better immunotherapeutic response. Furthermore, many common chemotherapeutic drugs were more effective for low-risk patients.

Conclusions: In conclusion, we developed a novel LRLPS for BC that could predict the prognosis, immune landscape, and treatment response.

Introduction

Breast cancer (BC) is the most common tumor and ranks fifth in cancer-related death globally[1]. Although early detection, diagnosis, and treatment for BC have made significant progress, cancer recurrence, distant metastasis, and drug resistance are still prevalent in patients with BC[2]. Many stratification terms have been built for the precise treatment of diseases, and polygenic makers may be more accurate than conventional methods[3]. BC is most commonly classified into five subtypes using PAM50, including luminal A, luminal B, HER2-enriched, normal-like, and basal-like[4]. However, the considerably heterogeneous nature of tumors limits the broad applicability of typing to some extent[5]. It is essential to investigate new potential markers for prognostic prediction and provide patients with personalized treatments.

Lactate is the endpoint of anaerobic glycolysis and usually is considered an endpoint or waste metabolite in cancer. Recent studies indicate that lactate is an essential regulator of cancer development, maintenance, tumor microenvironment, and metastasis[6, 7]. In breast cancer, GPR81 is upregulated and promotes tumor growth by releasing lactate from tumor cells[8]. Lactate dehydrogenase A might be a prognostic marker in clear cell renal cell carcinoma[9]. Lactate/BDNF/TrkB signaling could mediate epithelial-stroma interaction and lead to anlotinib resistance in gastric cancer[10]. In addition, lactate takes part in epigenetic regulation. Histone lysine lactylation is involved in regulating gene transcription[11].

Numerous studies have demonstrated that lactate is relevant to the tumor immune microenvironment (TIME) and immunotherapy. Elevated lactate levels are the primary cause of tumor microenvironment (TME) acidosis, which suppress CD8 + and CD4 + effector T cell function, and favor immunosuppressive Treg development[12–14]. As to Innate immunity, tumor-associated macrophages (TAMs) could subvert anti-tumor immune responses and act as a negative prognostic marker[15]. Lactate could promote transcriptional polarization of TAM towards the tumor-promoting M2 phenotype in cervical[16], breast[17], lung cancer and melanoma[18]. In addition to surgery, chemotherapy, radiotherapy and targeted therapies, immunotherapy is the fifth element of cancer treatment. However, the immunosuppressive heavy tumor microenvironment often limits immunotherapy and other therapeutic efficacy. Studies have found that elevated lactate levels can affect the therapeutic efficacy and overall survival of immune checkpoint inhibitors for melanoma[19], esophageal squamous cell carcinoma[20], and non-small cell lung cancer[21].

LncRNA consists of the RNA molecules with at least 200 base pairs that originate from the non-coding region of the genome, involved in almost all human biological processes and series of diseases[22–24]. Several studies have reported that lncRNAs could regulate lactate metabolism and immune status in different cancers. The lncRNA SNHG5 regulates BACH1 via miR-299 to promote glycolysis and proliferation in breast cancer cells[25]. LncRNA NEAT1-associated aerobic glycolysis in prostate cancer could blunt tumor immunosurveillance by T cells[26]. Furthermore, lncRNAs could be used as novel immunotherapeutic tools against cancer, and immunotherapy based on lncRNAs could increase the effectiveness and reduce off-target effects[27]. Together, lncRNA plays a role in diagnosing, prognosis, and treating BC[28].

Research has shown the critical value of lactate and lncRNAs in cancer classification, prognosis, and immunotherapy[29–31]. However, lactate-related lncRNAs have not been well studied in BC. Our study developed and verified an LRLPS to predict BC patients' prognosis, immune infiltration and therapeutic response by applying bioinformatics. As a result, our findings may provide new clues for cancer prognosis evaluation and treatment guidance.

Materials And Methods

2.1. Data Collection

The R package “TCGAbiolinks” was used to acquire the transcriptome profiling, simple nucleotide variations, and the clinical information of TCGA-BRCA patients[32]. We excluded male patients and remained 1096 BC samples and 112 normal samples. 916 patients with the OS > 30 days were included in the prognostic analysis. They were randomly divided into the training (n = 458) and test (n = 458) cohorts at a 1:1 ratio using the “caret” R package. Clinical characteristics of the three cohorts were analyzed with the “tableone” R package (Table S1). In the subsequent clinicopathological correlation analysis, we excluded patients with incomplete information. We acquired 284 lactate-related genes by querying the Molecular Signatures Database with “lactic” as the search keyword (Table S2)[33].

2.2. Identification of Differential Expressed LRLs in BC

The “EdgeR” R package assessed the differentially expressed lncRNAs and lactate-related genes ($P < 0.05$, $|log2FC|=1$). We retained differential expression lncRNAs expressed in more than half of the patients for further study. Further identification of lactate-related lncRNAs was performed with Pearson correlation analysis at a standard of $|R| > 0.4$ and the p-value < 0.001.

2.3. Construction and Validation of the LRLPS

The univariate Cox regression analysis identified the prognostic LRLs in the training cohort. We performed LASSO with the R package “glmnet” to avoid overfitting[34]. Then, the LRLPS was built with the multivariate Cox regression analysis based on the stepwise Akaike information criterion (stepAIC) value. According to the LRLPS, each sample could get the risk score with the following formula: Risk score = $\Sigma(Exp * Coef)$. The Coef and Exp were the coefficients and the expression level of each lncRNA, respectively. The high- and low-risk groups were divided according to the median risk score of the training cohort. We further performed the Kaplan–Meier survival analysis, time-dependent ROC curves, and univariate and multivariate analyses to evaluate the accuracy and independence of the LRLPS in prognosis prediction in the three cohorts.

2.4. Stratified analysis and Construction of the nomogram

The stratified analysis could assess the prognosis value of LRLPS in different subgroups stratified by several clinical features, including age, pathologic stage, T stage, N stage, M stage, ER, PR, and HER2 statuses. We constructed the nomogram with the independent prognostic factors. Nomogram accuracy was evaluated through ROC curves, C-index, and calibration curves. Finally, we measured the net benefit of using a nomogram and other clinical features alone based on decision curve analysis (DCA).

2.5. Functional Enrichment Analysis

We identified the differentially expressed genes (DEGs) between the two risk groups and annotated their functions with Gene Ontology (GO) and Kyoto Encyclopedia of Genes and Genomes (KEGG) using the R package “ClusterProfiler”[35]. The variations of pathway activity of the subgroups were further revealed with Gene Set Enrichment Analysis (GSEA) ($p < 0.05$ and FDR < 0.25)[36]. Annotated gene set “c2.cp.kegg.v7.5.1.symbols.gmt” could acquire from the MSigDB (https://www.gsea-msigdb.org/gsea/msigdb/).

2.6. Evaluation of immune infiltration and immunotherapy response in the two risk groups

We evaluated the proportion of tumor-infiltrating immune cells through the CIBERSORT algorithm[37]. Tumor purity, immune, stromal, and estimate scores were evaluated through the ESTIMATE algorithm[38]. Furthermore, we assessed twenty-seven potential immune checkpoints (ICPs) in the two risks groups. In order to predict immune checkpoint inhibitor (ICI) responses, we applied IPS and TIDE. TIDE was an online analysis that could predict the response to ICIs (http://tide.dfci.harvard.edu/)[39, 40]. The IPS is a machine learning-based system, it is scored as z scores according to four immunogenicity-related cell types (effector cells, immunosuppressive cells, MHC molecules, and immunomodulators), and it was positively correlated with immunogenicity[41]. It is reported that IPS could assess the tumor immunogenicity and response to ICI therapy in various tumor types. The IPS of BC patients were downloaded from The Cancer Immunome Atlas (TCIA) (https://tcia.at/home).

2.7. Correlation between the Risk Score and Tumor Mutation

The mutation landscapes in the two risk groups were analyzed with the “maftools” R package. Mutations in the genome per million bases are known as the tumor mutational burden (TMB), a potential immunotherapy biomarker[42, 43]. We evaluated the TMB in the two risk groups and explored the association between TMB and the risk score.

2.8. Evaluation of the Drug Sensitivity and Potential Target Drugs

The “pRRophetic” R package was used to calculate the half-maximal inhibitory concentrations (IC50) of the common chemotherapy drugs based on the Genomics of Drug Sensitivity in Cancer (GDSC; https://www.cancerrxgene.org/) database[44, 45]. As to the lncRNAs in the LRLPS, we explored the potential target drugs (approved by the FDA and those in clinical tests) with the CellMiner database (https://discover.nci.nih.gov/cellminer) [46, 47]. The relationship between model lncRNAs and drug sensitivity was studied using Pearson correlation analysis.

2.9. Statistical Analysis

We applied R software (version 4.0.5, https://www.r-project.org/) for all statistical analyses. P-value < 0.05 was set as statistically significant, and the significance levels were set as * $p \leq 0.05$, ** $p \leq 0.01$, *** $p \leq 0.001$ and ns = $p > 0.05$.

Results

3.1. Identification of the Differentially Expressed LRLs in BC Patients

There were 30 differentially expressed lactate-related genes and 4256 differentially expressed lncRNAs, respectively (Figs. 1A-B). Based on Pearson correlation analysis, we identified 196 differentially expressed LRLs for further investigation. Figure 1C showed the interaction between the lactate-related genes and LRLs.

3.2. Development and Evaluation of the LRLPS

In the training cohort, 17 LRLs with prognostic values were identified with the univariate Cox regression analysis (Fig. 2A). We performed LASSO cox analysis and identified 14 LRLs to avoid overfitting the model (Fig. 2B-C). The multivariate Cox regression analysis identified 7 LRLs to construct the LRLPS based on the lowest AIC 507.17 (Fig. 2D). Each patient would acquire a risk score by calculating the following: risk score= (1.915272666 * C9orf163) + (-0.677100153 * RP1-28O10.1) + (-0.503780886 * RP11-496I9.1) + (1.048467864 * CTD-3065J16.9) + (-0.692769124 * USP30-AS1) + (-0.835154753 * LINC01569) + (-1.077081426 * RP11-707G18.1) (Table S3). Subsequently, we evaluated the ability of the LRLPS in prognosis predicting. Kaplan-Meier analysis showed that patients in the high-risk group had shorter overall survival (OS) (Fig. 2E). The area under the 3-, 5-, 10-year time-dependent ROC curves (AUC) were 0.7536, 0.7229, and 0.7703, respectively, which indicated the accuracy of the LRLPS (Fig. 2F). Figure 2G indicated the correlation between the risk score and the outcome of BC patients. Figure 2H indicated that the AUC of risk score was the highest (0.749), followed by the N stage (0.663) and pathological stage (0.649). The univariate (Fig. 2I) and multivariate (Fig. 2J) Cox regression analyses indicated the independent prognostic value of the risk score.

3.3. Validation of the LRLPS

To assess the stability of the LRLPS, we used the same analyses in the test and entire cohorts. High-risk patients always had a worse OS than low-risk patients in the two cohorts (Figs. 3A, 3D). The AUCs of the 3-, 5-, and 10-year ROC curves were 0.7284, 0.6964, and 0.6716 in the test cohort (Fig. 3B), and 0.7484, 0.7111, 0.7179 in the entire cohort (Fig. 3E). Figures 3C and 3F indicated that the higher risk score was correlated with increased mortality. In the test cohort, the AUC of the risk score was the highest (0.761) (Fig. 3G). The risk score was an independent prognostic factor in the multivariate Cox regression analysis but not a statistically significant independent prognostic according to the univariate Cox regression analysis (Figs. 3H-I). In the entire cohort, the risk score had the highest AUC (0.752) and was an independent prognostic factor (Figs. 3J-L). To further explore whether the signature was suitable for different clinical subgroups, we performed the stratification and Kaplan-Meier survival analyses. There were always significant differences in survival between the two risk groups in all clinical subgroups (Fig. 4A-Q). The results indicated that the prognostic signature was accurate, independent, and widely applicable.

3.4. Construction and Evaluation of the Nomogram

In order to make our model better assist clinical decision-making, we constructed a nomogram that could predict the 3-, 5-, and 10-year survival probability (Fig. 5A). The nomogram's 3-, 5- and 10-year AUCs were 0.7570, 0.7196 and 0.6237, indicating the reliability (Fig. 5B). The calibration curves proved that our prognostic nomogram could accurately predict the survival probabilities (Figs. 5C–E). Furthermore, DCA curves indicated that the nomogram was associated with more benefits to BC patients than other clinicopathological factors (Figs. 5F-G).

3.5 Function analyses

We used GO/KEGG and GSEA analyses to analyze the functions of the two risk groups. There were 3962 DEGs between the two-risk groups, including 1524 up-regulated genes and 2168 down-regulated genes for the high-risk group. GO analysis showed that these DEGs participated in many biological processes, such as humoral immune response, lymphocyte-mediated immunity, and epidermis development (Fig. 6A). They could act as structural constituents in the T cell receptor complex, plasma membrane signaling receptor complex, and immunoglobulin complex and play an essential part in receptor ligand activity, signaling receptor activator activity, and gated channel activity (Fig. 6A). KEGG analysis showed that the down-regulated genes were related to PD-L1 expression, primary immunodeficiency, cytokine-cytokine receptor interaction, and PD-1 checkpoint pathway in cancer (Fig. 6B). Through GSEA analysis, we further observed the variations of pathway activity between the two risk groups. The low-risk group was enriched with the classical immune-related pathways, such as T/B cell receptor signaling pathways, leukocyte transendothelial migration, and antigen processing and presentation, while the high-risk group was enriched with the cell cycle-related pathways, including cell cycle, DNA replication, and mismatch repair (Fig. 6C).

3.6. Differential immune infiltration and immunotherapy response in the two groups

To further study the immune landscape, we performed CIBERSORT and ESTIMATE algorithms. The heat map demonstrated the levels of the immune infiltrating cells in the two risk groups (Fig. 7A). The macrophages M0, M2, and NK cells resting were the main components in the high-risk group; However, the resting CD4 T memory cells, CD8 T cells, naive B cells, activated dendritic cells, monocytes, and gamma delta T cells were mainly in the low-risk group (Fig. 7B). The ESTIMATE results showed that high-risk patients had lower stromal and immune scores but had higher tumor purity (Fig. 7C). Furthermore, the risk score was negatively associated with the stromal and immune scores while positively associated with tumor purity (Fig. 7D). ICP was proved related to immunotherapy[48]. We assessed the expression levels of 27 ICPs in the two risk groups. They all expressed much higher in the low-risk group, such as CTLA4, HAVCR2, TIGIT, PDCD1 and LAG3 (Fig. 7E). TIDE could identify the patients' response to ICIs. As shown in Fig. 7F, the low-risk group had a significantly higher response rate to immunotherapy. The risk

score for non-responders to immunotherapy tended to be much higher than that for responders (Fig. 7G). Furthermore, all four types of IPS were higher in the low-risk group, indicating that the low-risk patients could acquire more benefits from ICIs (Figs. 7H-K). These results indicated that the low-risk group with the immune signature might have a better immunotherapy response.

In addition, we investigated whether the seven LRLs in our signature were associated with the immune signature. USP30-AS1 was significantly positively related to activated CD4 memory T cells, Macrophages M1 and CD8 T cells, and classic ICPs, such as PD-1 and CTLA4 (Figures S1A-B). These results indicated that USP30-AS1 might make a difference in the TIME.

3.7. Somatic Mutation analysis

The potential contribution of genomic changes to tumor immunity and immune infiltration has been explored in previous studies[49, 50]. Figures 8A-B showed the top 30 genes mutated most frequently in the two risk groups. Although the overall mutation frequency is similar between the two groups (high versus low, 89.49 versus 92.12%), about one-third of the genes are different between the groups. SPTA1, APOB, ARID1A, BIRC6, GSMD3, RELN, RYR3, LRP1, and HUWE1 were not observed in the low-risk group. Regarding the most common BRCA biomarkers, the high-risk group had significantly more patients with TP53 mutations (low versus high, 25.6 versus 40.8%) (Fig. 8C). A higher mutation frequency of PIK3CA was observed in the low-risk group (low versus high, 39.7 versus 26.7%) (Fig. 8D). Further, the TMB in the high-risk group was significantly higher (P = 0.035) (Fig. 8E). The Pearson correlation analysis indicated the positive correlation between TMB and the risk score (Fig. 8F).

3.8. Prediction of potential drugs and the sensitivity of chemotherapeutic agents

To further explore effective drugs for BC patients to guide precision treatment, we analyzed the sensitivity to common chemotherapeutic agents of the two risk groups. High-risk patients had higher IC50 of 5-Fluorouracil, Sorafenib, Tamoxifen, Temozolomide, Temsirolimus, and Vinblastine (Figs. 9A-F), indicating they were more likely to be resistant to the above drugs. Furthermore, we explored the potential drugs targeted to the seven model genes with the CellMiner database. We finally acquired 16 gene-drug correlations, of which 11 correlations pointed to the USP30-AS1, and five correlations pointed to the C9orf163 (Fig. 9G). C9orf163 expressed higher in the high-risk group, while C9orf163 expressed higher in the low-risk group. Ribavirin, Fulvestrant, SR16157, 8-Chloro-adenosine, and Methylprednisolone were positively related to C9orf163, so they might benefit high-risk patients. Conversely, the BRCA drug Ifosfamide was positively correlated with USP30-AS1; it might benefit the low-risk patients (Fig. 9G).

Discussion

BC has the highest incidence rate among all cancers globally, which causes tens of thousands of female deaths every year[4]. BC is characterized by tumor heterogeneity at the molecular level of tumor cells and

the tumor microenvironment (TME)[51, 52]. Tumor heterogeneity complicates the aggressiveness and treatment of BC[53]. Recent studies have revealed lactate's diverse roles in the TME. Although cancer cells have a sufficient oxygen supply, they still use glucose and produce lactate excessively, which could cause acidosis, angiogenesis, and immunosuppression[54]. In BC, lactate is correlated with the resistance to PI3K inhibitors[55]. In several cancers, lactate is essential in predicting prognosis, tumor microenvironment, and immune response[29, 30, 56]. However, the prognostic value of lactate in BC remains largely unknown. This is the first study investigating the role of lactate in predicting prognosis, immune status, and therapeutic response in BC.

We first identified 196 differential expression LRLs for further study. We used the univariate Cox regression analysis, LASSO, and multivariate Cox regression analysis to construct the LRLPS. Survival analysis and the time-dependent ROC curves confirmed the prognostic value and reliability of the LRLPS. The AUC of the risk score was higher than other clinicopathological characteristics, indicating the highest prognostic performance of the LRLPS. Subsequent univariate and multivariate Cox regression analyses further indicated the independent prognostic predict ability of the risk score. Stratified analysis showed that the LRLPS was suitable for patients in any clinical subgroups. Furthermore, the nomogram provided a powerful tool for clinicians to make decisions.

The GO/KEGG and GSEA indicated that the immune-related pathways differed between the two-risk groups. Previous research has demonstrated that lactate could regulate TMB. Through its ability to enhance the metabolic profile of the Treg and maintain acidity in the TME, lactate could enhance the immunosuppressive effect[57]. Excessive lactate inhibits T-cell proliferation, such as Natural killer, dendritic, and CD8 + T cells[58–60]. In addition, lactate could potentiate the anti-inflammatory effects by activating macrophages, promoting angiogenesis, tissue remodeling, and finally accelerating tumor growth and invasion[60]. Hence, we further explore the TIME through several algorithms. Tumor immune cell infiltration (TIICs) is a crucial component of the TIME. We calculated the levels of TIICs in BC with CIBERSORT. The high-risk group was enriched with the immunosuppressive immune cells, such as macrophages M0 and M2, which were also the critical members of EMT and cancer metastasis[61, 62]. Instead, CD4/8$^+$ T cells, the vital factors in killing tumors and promoting immune response, were the main component in the low-risk group[41]. According to the ESTIMATE analysis, the low-risk group had a higher immune score and stromal content while lower tumor purity than the high-risk group.

Immunotherapy has been a new treatment modality in BC, especially for metastatic BC[63]. We further estimated the immunotherapy responses of the two risk groups. It is reported that ICIs antitumor relay on the CD8 + T cells, CD4 + T cells, and dendritic cells[64, 65]. The immune cell infiltration levels were positively correlated with the responsiveness to ICIs[66, 67]. As an essential biomarker for predicting cancer immunotherapy[68], the 27 ICPs expressed higher in the low-risk group. Therefore, we speculated that the low-risk group could respond better to immunotherapy and further verified the conclusion through TIDE and IPS analyses. All IPSs of CTLA4-/PD-1-, CTLA4 + /PD-1-, CTLA4-/PD-1 +, and CTLA4+/PD-1 + were higher in the low-risk group, indicted that the low-risk group had a better response to immunotherapy.

Patients with high risk had the higher TMB in our study. Some research has indicated that TMB could act as a biomarker for predicting the response to ICIs[42, 43]. However, the predictive value varies among different cancers and might be insufficient in solid tumors[69]. Thus, ICIs could benefit low-risk patients, while other immunotherapy might be appropriate for high-risk patients. These results indicated the significant differences in the degree of immune cell infiltration and immunotherapy response between the two risk groups identified by lactate-related signature.

Regarding the seven LRLs in our signature, some have been studied before in other cancers. USP30-AS1 is involved in autophagy, proliferation, and apoptosis in acute myeloid leukemia, glioblastoma, and cervical cancer[70–72]. In our study, USP30-AS1 was positively correlated with the antitumor immune cells and the classic ICPs. These results indicated the potential role of USP30-AS1 in TME. C9orf163 could develop the tumor microenvironment through cytokine and chemokine signaling and might act as a tumor suppressor in anaplastic gliomas and pancreatic cancer[73, 74]. However, more research is required to clarify the molecular mechanism of the seven LRLs in BC.

In treating BC, chemotherapeutic drugs could reduce the tumor recurrence rate and be a primary treatment option for metastatic disease. However, chemo-resistance severely limited the clinical efficacy of chemotherapeutic drugs for BC patients[75]. Thus, we assessed the BC patients' response to chemotherapy with the IC50 value. The pRRophetic showed that low-risk patients were more sensitive to the common chemotherapy drugs, such as 5-Fluorouracil, Sorafenib, Tamoxifen, Temozolomide, Temsirolimus, and Vinblastine. Furthermore, we performed the CellMiner database to predict the candidate small-molecule compounds. The results indicated that Ribavirin, Fulvestrant, SR16157, 8-Chloro-adenosine, and Methylprednisolone might benefit patients with high risk. In combination, these discoveries may provide BC patients with suitable treatment options.

However, there were still a few limitations to our study. We used the TCGA dataset for all analyses since other databases lacked the needed LRLs data, including the Gene Expression Omnibus (GEO) and METABRIC databases, which prevented us from verifying the results. Therefore, it is better to validate in a prospective cohort. Secondly, further studies on the biological functions of the seven LRLs are needed to be performed in vivo and in vitro.

Conclusions

Altogether, a novel lactate-related lncRNAs prognostic signature was identified for BC patients in this study, which could predict the prognosis and immune infiltration. The LRLPS also provided an effective method for personalized risk estimation and assessment of treatment response to immunotherapy and chemotherapy, which may be clinically helpful. Finally, the seven LRLs could become potential treatment targets for BC.

Abbreviations

BC Breast cancer

LncRNA Long non-coding RNA

LRLPS Lactate-related lncRNAs prognostic signature

LRLs Lactate-related lncRNAs

LASSO least absolute shrinkage and selection operator

ROC receiver operating characteristic

TIDE Tumor Immune Dysfunction and Exclusion

IPS Immunophenoscore

GSEA Gene set enrichment analysis

TIME Tumor immune microenvironment

DCA Decision curve analysis

DEGs Differentially expressed genes

GO Gene Ontology

KEGG Kyoto Encyclopedia of Genes and Genomes

ICPs Immune checkpoints

TMB Tumor mutational burden

IC50 Half-maximal inhibitory concentrations

OS Overall survival

AUC Area under ROC curve

TCGA The Cancer Genome Atlas

FDR False discovery rate

Declarations

Ethics approval and consent to participate

Not applicable

Consent for publication

Not applicable

Availability of data and materials

The data can be found here: https://portal.gdc.cancer.gov/repository.

Authors' contributions

YBZ, JL, CFL conceptualized and designed the study. CF, HZW, WWW, and HQ prepared the dataset. YFC and YZ, YWJ analyzed and interpreted the data. FW and XL wrote and reviewed the manuscript. SQZ supervised the study. All authors contributed to the article and approved the submitted version.

Funding

This work is supported by National Natural Science Foundation of China 82103212.

Competing interests

The authors declare that they have no competing interests

Acknowledgments

We thank the TCGA database for providing the original study data.

References

1. HARBECK N, GNANT M. Breast cancer [J]. Lancet, 2017, 389(10074): 1134–50.
2. JABBARZADEH KABOLI P, SALIMIAN F, AGHAPOUR S, et al. Akt-targeted therapy as a promising strategy to overcome drug resistance in breast cancer - A comprehensive review from chemotherapy to immunotherapy [J]. Pharmacol Res, 2020, 156: 104806.
3. LI J, LIU C, CHEN Y, et al. Tumor Characterization in Breast Cancer Identifies Immune-Relevant Gene Signatures Associated With Prognosis [J]. Front Genet, 2019, 10: 1119.
4. HARBECK N, PENAULT-LLORCA F, CORTES J, et al. Breast cancer [J]. Nat Rev Dis Primers, 2019, 5(1): 66.
5. WAKS A G, WINER E P. Breast Cancer Treatment: A Review [J]. JAMA, 2019, 321(3): 288–300.
6. DOHERTY J R, CLEVELAND J L. Targeting lactate metabolism for cancer therapeutics [J]. J Clin Invest, 2013, 123(9): 3685–92.
7. HAYES C, DONOHOE C L, DAVERN M, et al. The oncogenic and clinical implications of lactate induced immunosuppression in the tumour microenvironment [J]. Cancer Lett, 2021, 500: 75–86.

8. LONGHITANO L, FORTE S, ORLANDO L, et al. The Crosstalk between GPR81/IGFBP6 Promotes Breast Cancer Progression by Modulating Lactate Metabolism and Oxidative Stress [J]. Antioxidants (Basel), 2022, 11(2).
9. GIRGIS H, MASUI O, WHITE N M, et al. Lactate dehydrogenase A is a potential prognostic marker in clear cell renal cell carcinoma [J]. Mol Cancer, 2014, 13: 101.
10. JIN Z, LU Y, WU X, et al. The cross-talk between tumor cells and activated fibroblasts mediated by lactate/BDNF/TrkB signaling promotes acquired resistance to anlotinib in human gastric cancer [J]. Redox Biol, 2021, 46: 102076.
11. IZZO L T, WELLEN K E. Histone lactylation links metabolism and gene regulation [J]. Nature, 2019, 574(7779): 492–3.
12. CORBET C, FERON O. Tumour acidosis: from the passenger to the driver's seat [J]. Nat Rev Cancer, 2017, 17(10): 577–93.
13. ERRA DíAZ F, DANTAS E, GEFFNER J. Unravelling the Interplay between Extracellular Acidosis and Immune Cells [J]. Mediators Inflamm, 2018, 2018: 1218297.
14. NAKAGAWA Y, NEGISHI Y, SHIMIZU M, et al. Effects of extracellular pH and hypoxia on the function and development of antigen-specific cytotoxic T lymphocytes [J]. Immunol Lett, 2015, 167(2): 72–86.
15. GABRILOVICH D I, OSTRAND-ROSENBERG S, BRONTE V. Coordinated regulation of myeloid cells by tumours [J]. Nat Rev Immunol, 2012, 12(4): 253–68.
16. STONE S C, ROSSETTI R A M, ALVAREZ K L F, et al. Lactate secreted by cervical cancer cells modulates macrophage phenotype [J]. J Leukoc Biol, 2019, 105(5): 1041–54.
17. MU X, SHI W, XU Y, et al. Tumor-derived lactate induces M2 macrophage polarization via the activation of the ERK/STAT3 signaling pathway in breast cancer [J]. Cell Cycle, 2018, 17(4): 428–38.
18. ZHANG D, TANG Z, HUANG H, et al. Metabolic regulation of gene expression by histone lactylation [J]. Nature, 2019, 574(7779): 575–80.
19. KELDERMAN S, HEEMSKERK B, VAN TINTEREN H, et al. Lactate dehydrogenase as a selection criterion for ipilimumab treatment in metastatic melanoma [J]. Cancer Immunol Immunother, 2014, 63(5): 449–58.
20. WANG X, ZHANG B, CHEN X, et al. Lactate dehydrogenase and baseline markers associated with clinical outcomes of advanced esophageal squamous cell carcinoma patients treated with camrelizumab (SHR-1210), a novel anti-PD-1 antibody [J]. Thorac Cancer, 2019, 10(6): 1395–401.
21. ZHANG Z, LI Y, YAN X, et al. Pretreatment lactate dehydrogenase may predict outcome of advanced non small-cell lung cancer patients treated with immune checkpoint inhibitors: A meta-analysis [J]. Cancer Med, 2019, 8(4): 1467–73.
22. FATICA A, BOZZONI I. Long non-coding RNAs: new players in cell differentiation and development [J]. Nat Rev Genet, 2014, 15(1).
23. HAUPTMAN N, GLAVAČ D. Long non-coding RNA in cancer [J]. Int J Mol Sci, 2013, 14(3): 4655–69.

24. ESTELLER M. Non-coding RNAs in human disease [J]. Nat Rev Genet, 2011, 12(12): 861–74.
25. HUANG S-L, HUANG Z-C, ZHANG C-J, et al. LncRNA SNHG5 promotes the glycolysis and proliferation of breast cancer cell through regulating BACH1 via targeting miR-299 [J]. Breast Cancer, 2022, 29(1): 65–76.
26. XIA K-G, WANG C-M, SHEN D-Y, et al. LncRNA NEAT1-associated aerobic glycolysis blunts tumor immunosurveillance by T cells in prostate cancer [J]. Neoplasma, 2022.
27. KAUR M, KAUR B, KONAR M, et al. Noncoding RNAs as novel immunotherapeutic tools against cancer [J]. Adv Protein Chem Struct Biol, 2022, 129: 135–61.
28. RODRíGUEZ BAUTISTA R, ORTEGA GóMEZ A, HIDALGO MIRANDA A, et al. Long non-coding RNAs: implications in targeted diagnoses, prognosis, and improved therapeutic strategies in human non- and triple-negative breast cancer [J]. Clin Epigenetics, 2018, 10: 88.
29. XIE Y, ZHANG J, LI M, et al. Identification of Lactate-Related Gene Signature for Prediction of Progression and Immunotherapeutic Response in Skin Cutaneous Melanoma [J]. Front Oncol, 2022, 12: 818868.
30. SUN Z, TAO W, GUO X, et al. Construction of a Lactate-Related Prognostic Signature for Predicting Prognosis, Tumor Microenvironment, and Immune Response in Kidney Renal Clear Cell Carcinoma [J]. Front Immunol, 2022, 13: 818984.
31. XU S, XIE J, ZHOU Y, et al. Integrated Analysis of RNA Binding Protein-Related lncRNA Prognostic Signature for Breast Cancer Patients [J]. Genes (Basel), 2022, 13(2).
32. COLAPRICO A, SILVA T C, OLSEN C, et al. TCGAbiolinks: an R/Bioconductor package for integrative analysis of TCGA data [J]. Nucleic Acids Res, 2016, 44(8): e71.
33. LIBERZON A, BIRGER C, THORVALDSDóTTIR H, et al. The Molecular Signatures Database (MSigDB) hallmark gene set collection [J]. Cell Syst, 2015, 1(6): 417–25.
34. FRIEDMAN J, HASTIE T, TIBSHIRANI R. Regularization Paths for Generalized Linear Models via Coordinate Descent [J]. J Stat Softw, 2010, 33(1).
35. YU G, WANG L-G, HAN Y, et al. clusterProfiler: an R package for comparing biological themes among gene clusters [J]. OMICS, 2012, 16(5): 284–7.
36. SUBRAMANIAN A, KUEHN H, GOULD J, et al. GSEA-P: a desktop application for Gene Set Enrichment Analysis [J]. Bioinformatics, 2007, 23(23): 3251–3.
37. NEWMAN A M, LIU C L, GREEN M R, et al. Robust enumeration of cell subsets from tissue expression profiles [J]. Nat Methods, 2015, 12(5): 453–7.
38. YOSHIHARA K, SHAHMORADGOLI M, MARTíNEZ E, et al. Inferring tumour purity and stromal and immune cell admixture from expression data [J]. Nat Commun, 2013, 4: 2612.
39. FU J, LI K, ZHANG W, et al. Large-scale public data reuse to model immunotherapy response and resistance [J]. Genome Med, 2020, 12(1): 21.
40. JIANG P, GU S, PAN D, et al. Signatures of T cell dysfunction and exclusion predict cancer immunotherapy response [J]. Nat Med, 2018, 24(10): 1550–8.

41. CHAROENTONG P, FINOTELLO F, ANGELOVA M, et al. Pan-cancer Immunogenomic Analyses Reveal Genotype-Immunophenotype Relationships and Predictors of Response to Checkpoint Blockade [J]. Cell Rep, 2017, 18(1): 248–62.
42. LU S, STEIN J E, RIMM D L, et al. Comparison of Biomarker Modalities for Predicting Response to PD-1/PD-L1 Checkpoint Blockade: A Systematic Review and Meta-analysis [J]. JAMA Oncol, 2019, 5(8): 1195–204.
43. SHUM B, LARKIN J, TURAJLIC S. Predictive biomarkers for response to immune checkpoint inhibition [J]. Semin Cancer Biol, 2022, 79.
44. GEELEHER P, COX N J, HUANG R S. Clinical drug response can be predicted using baseline gene expression levels and in vitro drug sensitivity in cell lines [J]. Genome Biol, 2014, 15(3): R47.
45. YANG W, SOARES J, GRENINGER P, et al. Genomics of Drug Sensitivity in Cancer (GDSC): a resource for therapeutic biomarker discovery in cancer cells [J]. Nucleic Acids Res, 2013, 41(Database issue): D955-D61.
46. SHANKAVARAM U T, REINHOLD W C, NISHIZUKA S, et al. Transcript and protein expression profiles of the NCI-60 cancer cell panel: an integromic microarray study [J]. Mol Cancer Ther, 2007, 6(3): 820–32.
47. SHANKAVARAM U T, VARMA S, KANE D, et al. CellMiner: a relational database and query tool for the NCI-60 cancer cell lines [J]. BMC Genomics, 2009, 10: 277.
48. TOPALIAN S L, DRAKE C G, PARDOLL D M. Immune checkpoint blockade: a common denominator approach to cancer therapy [J]. Cancer Cell, 2015, 27(4): 450–61.
49. THORSSON V, GIBBS D L, BROWN S D, et al. The Immune Landscape of Cancer [J]. Immunity, 2018, 48(4).
50. ROONEY M S, SHUKLA S A, WU C J, et al. Molecular and genetic properties of tumors associated with local immune cytolytic activity [J]. Cell, 2015, 160(1–2): 48–61.
51. SOUSA B, RIBEIRO A S, PAREDES J. Heterogeneity and Plasticity of Breast Cancer Stem Cells [J]. Adv Exp Med Biol, 2019, 1139.
52. BAKER J H E, KYLE A H, REINSBERG S A, et al. Heterogeneous distribution of trastuzumab in HER2-positive xenografts and metastases: role of the tumor microenvironment [J]. Clin Exp Metastasis, 2018, 35(7): 691–705.
53. JANUŠKEVIČIENĖ I, PETRIKAITĖ V. Heterogeneity of breast cancer: The importance of interaction between different tumor cell populations [J]. Life Sci, 2019, 239: 117009.
54. HO Y-J, CHU S-W, LIAO E-C, et al. Normalization of Tumor Vasculature by Oxygen Microbubbles with Ultrasound [J]. Theranostics, 2019, 9(24): 7370–83.
55. HILLIS A L, TOKER A. Lactate Lights up PI3K Inhibitor Resistance in Breast Cancer [J]. Cancer Cell, 2020, 38(4): 441–3.
56. MAI S, LIANG L, MAI G, et al. Development and Validation of Lactate Metabolism-Related lncRNA Signature as a Prognostic Model for Lung Adenocarcinoma [J]. Front Endocrinol (Lausanne), 2022,

13: 829175.
57. DASTMALCHI F, DELEYROLLE L P, KARACHI A, et al. Metabolomics Monitoring of Treatment Response to Brain Tumor Immunotherapy [J]. Front Oncol, 2021, 11: 691246.
58. HAAS R, SMITH J, ROCHER-ROS V, et al. Lactate Regulates Metabolic and Pro-inflammatory Circuits in Control of T Cell Migration and Effector Functions [J]. PLoS Biol, 2015, 13(7): e1002202.
59. GROTE S, UREñA-BAILéN G, CHAN K C-H, et al. In Vitro Evaluation of CD276-CAR NK-92 Functionality, Migration and Invasion Potential in the Presence of Immune Inhibitory Factors of the Tumor Microenvironment [J]. Cells, 2021, 10(5).
60. CERTO M, TSAI C-H, PUCINO V, et al. Lactate modulation of immune responses in inflammatory versus tumour microenvironments [J]. Nat Rev Immunol, 2021, 21(3): 151–61.
61. QIAN B-Z, POLLARD J W. Macrophage diversity enhances tumor progression and metastasis [J]. Cell, 2010, 141(1): 39–51.
62. BISWAS S K, MANTOVANI A. Macrophage plasticity and interaction with lymphocyte subsets: cancer as a paradigm [J]. Nat Immunol, 2010, 11(10): 889–96.
63. ADAMS S, GATTI-MAYS M E, KALINSKY K, et al. Current Landscape of Immunotherapy in Breast Cancer: A Review [J]. JAMA Oncol, 2019, 5(8): 1205–14.
64. SATO Y, BOLZENIUS J K, ETELEEB A M, et al. CD4 + T cells induce rejection of urothelial tumors after immune checkpoint blockade [J]. JCI Insight, 2018, 3(23).
65. FARHOOD B, NAJAFI M, MORTEZAEE K. CD8 cytotoxic T lymphocytes in cancer immunotherapy: A review [J]. J Cell Physiol, 2019, 234(6): 8509–21.
66. KüMPERS C, JOKIC M, HAASE O, et al. Immune Cell Infiltration of the Primary Tumor, Not PD-L1 Status, Is Associated With Improved Response to Checkpoint Inhibition in Metastatic Melanoma [J]. Front Med (Lausanne), 2019, 6: 27.
67. KARN T, JIANG T, HATZIS C, et al. Association Between Genomic Metrics and Immune Infiltration in Triple-Negative Breast Cancer [J]. JAMA Oncol, 2017, 3(12): 1707–11.
68. PATEL S P, KURZROCK R. PD-L1 Expression as a Predictive Biomarker in Cancer Immunotherapy [J]. Mol Cancer Ther, 2015, 14(4): 847–56.
69. XU Z, DAI J, WANG D, et al. Assessment of tumor mutation burden calculation from gene panel sequencing data [J]. Onco Targets Ther, 2019, 12: 3401–9.
70. ZHOU W, XU S, DENG T, et al. LncRNA USP30-AS1 promotes the survival of acute myeloid leukemia cells by cis-regulating USP30 and ANKRD13A [J]. Hum Cell, 2022, 35(1): 360–78.
71. CHEN M, CHI Y, CHEN H, et al. Long non-coding RNA USP30-AS1 aggravates the malignant progression of cervical cancer by sequestering microRNA-299-3p and thereby overexpressing PTP4A1 [J]. Oncol Lett, 2021, 22(1): 505.
72. WANG N, LI J, XIN Q, et al. USP30-AS1 contributes to mitochondrial quality control in glioblastoma cells [J]. Biochem Biophys Res Commun, 2021, 581: 31–7.

73. WANG W, YANG F, ZHANG L, et al. LncRNA profile study reveals four-lncRNA signature associated with the prognosis of patients with anaplastic gliomas [J]. Oncotarget, 2016, 7(47): 77225–36.
74. ZHUANG H, HUANG S, ZHOU Z, et al. A four prognosis-associated lncRNAs (PALnc) based risk score system reflects immune cell infiltration and predicts patient survival in pancreatic cancer [J]. Cancer Cell Int, 2020, 20: 493.
75. O'DRISCOLL L, CLYNES M. Biomarkers and multiple drug resistance in breast cancer [J]. Curr Cancer Drug Targets, 2006, 6(5): 365–84.

Figures

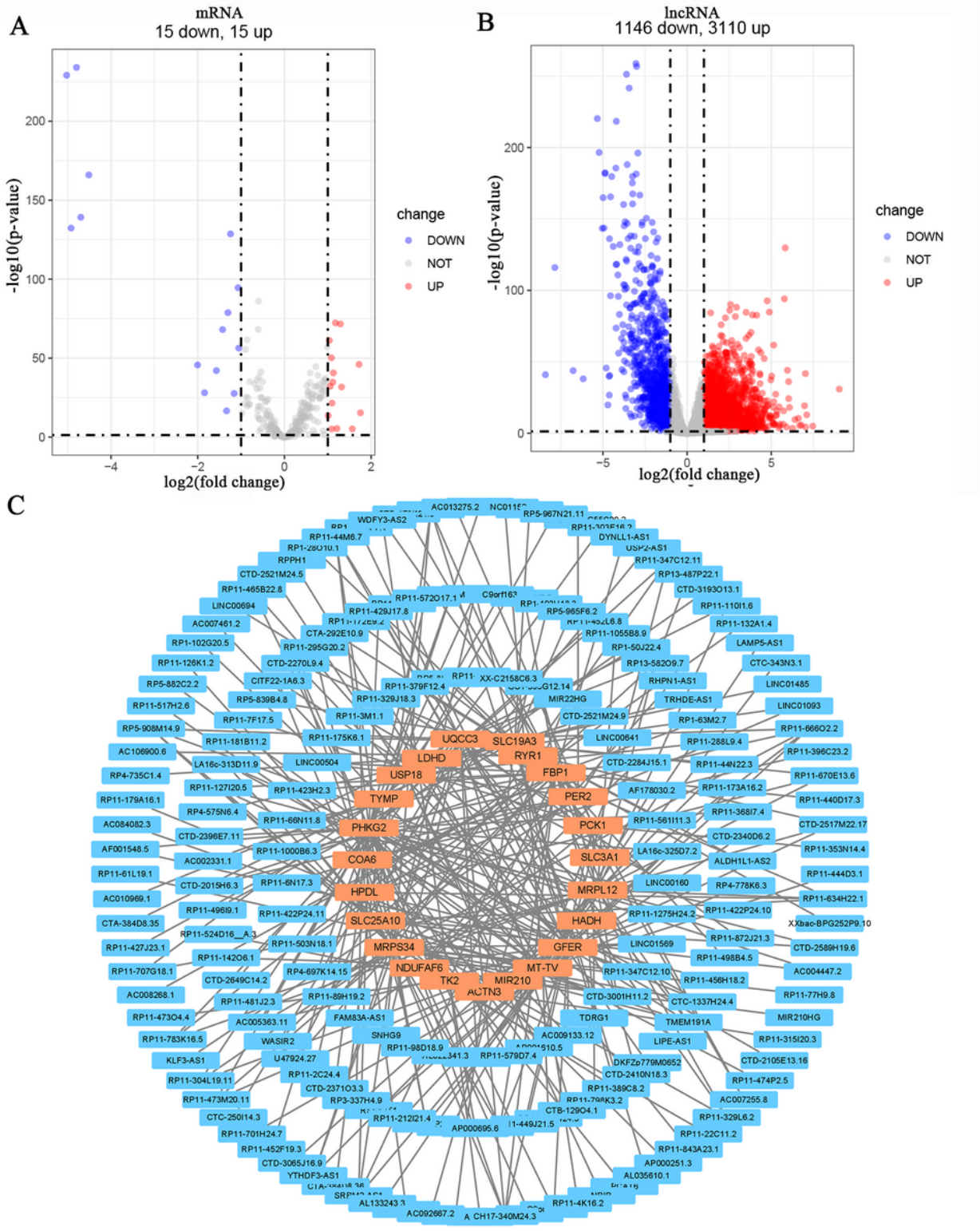

Figure 1

Identification of the differential expressed LRLs. The volcano plots of the differentially expressed lactate-related genes (A) and differentially expressed lncRNAs (B). (C) The interaction between the differentially expressed lactate-related genes and LRLs.

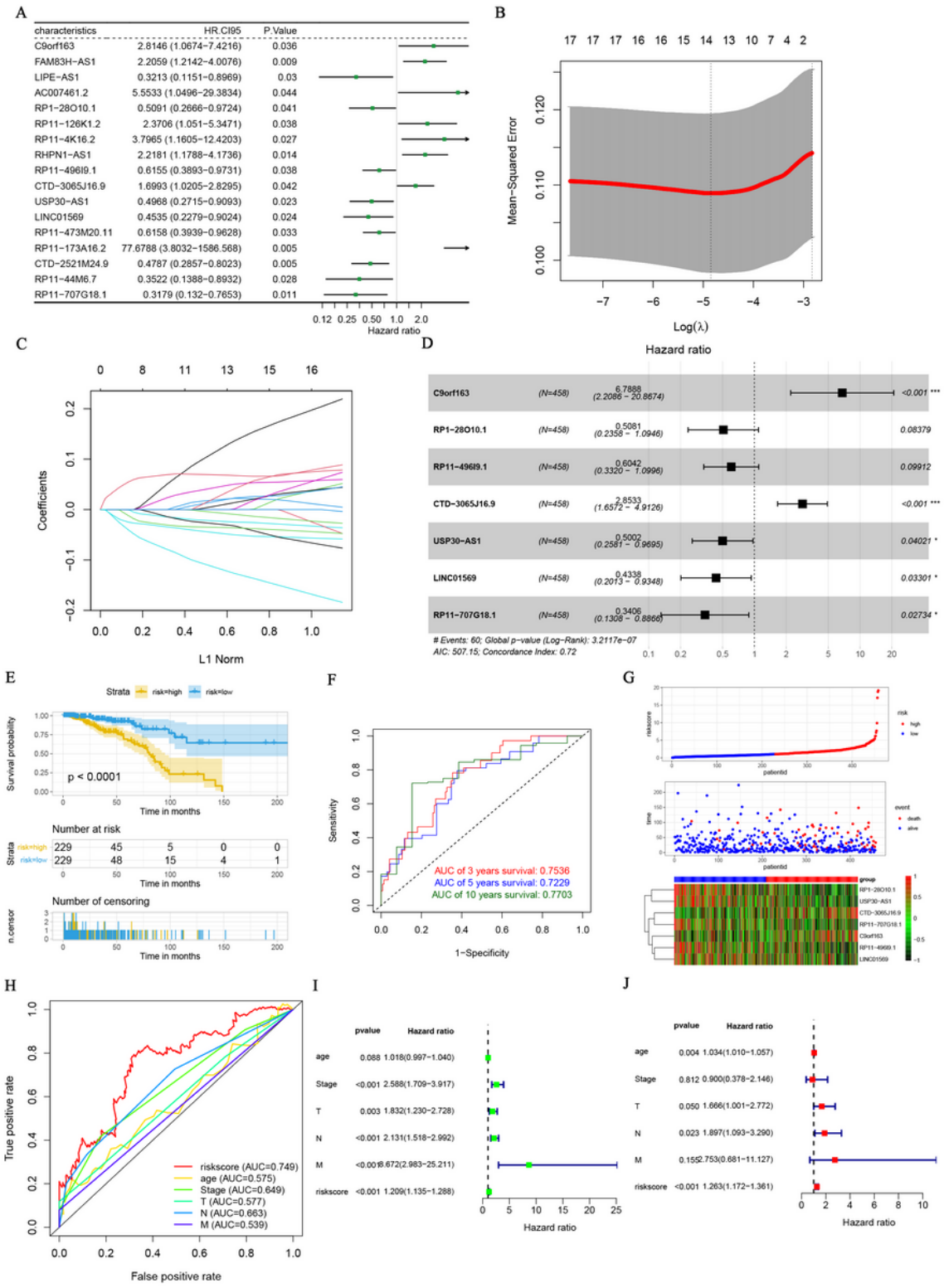

Figure 2

Construction and evaluation of the LRLPS. (A) The univariate Cox regression analysis of LRLs in the training cohort. (B) The cross-validation graph shows the optimal parameter selection with minimum criteria in the LASSO model. (C)The LASSO coefficient profiles of the 14 LRLs. (D) The forest graph showed the results of stepwise multivariable cox proportional hazards regression analysis. (E) The OS curve of the two risk groups. (F) The time-dependent ROC curves of the LRLPS. (G) The risk score, clinical

event, and the model genes in the two risk groups. (H) The ROC curves of the risk score and other clinicopathological parameters. The univariate(I) and multivariate (J) Cox regression analyses.

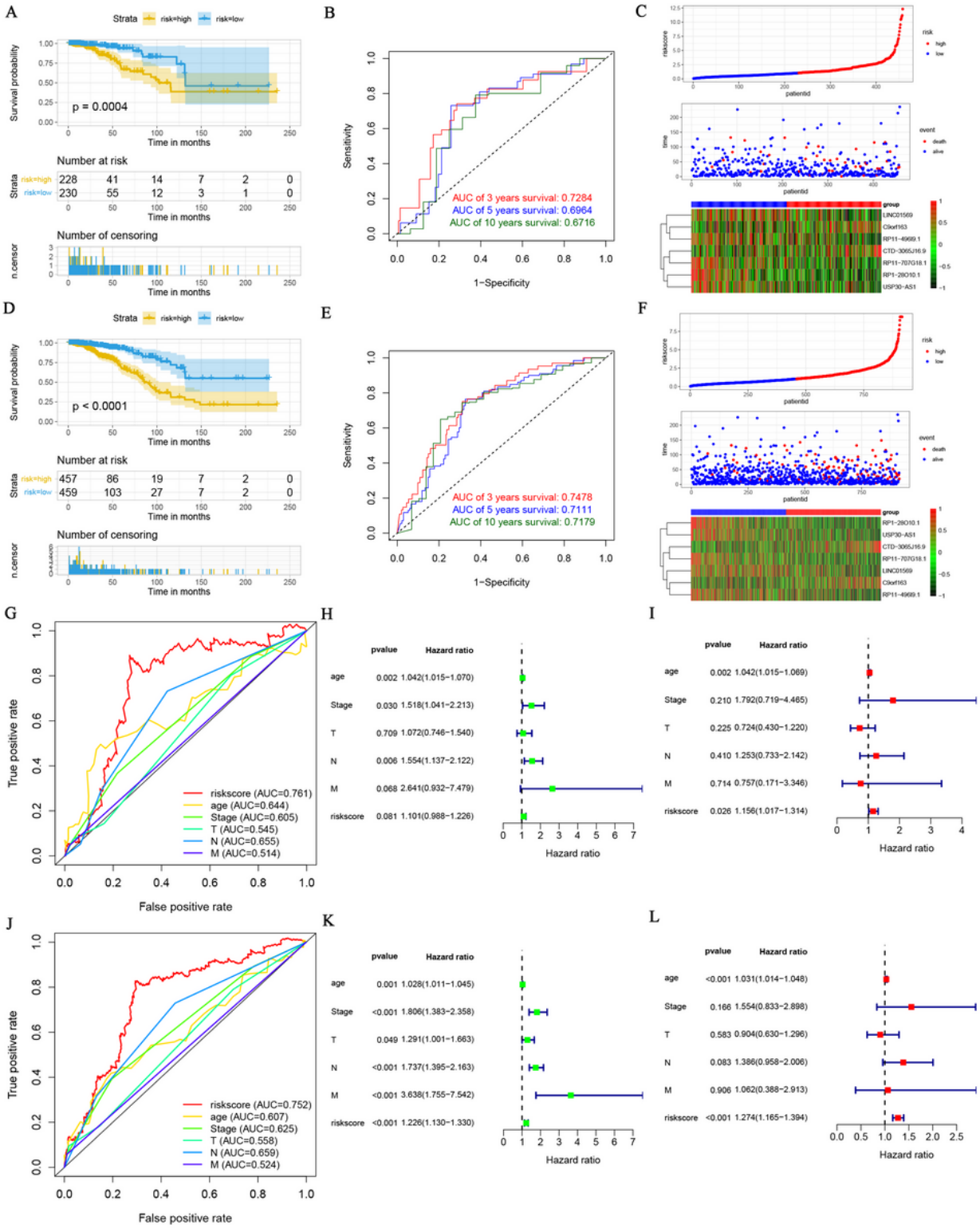

Figure 3

Validation of the LRLPS. The OS curve of the two risk groups in test (A) and entire (D) cohorts. The time-dependent ROC curves in test (B) and entire (E) cohorts. The risk score, clinical event, and the model

genes in the two risk groups in test (C) and entire (F) cohorts. The ROC curves of the risk score and other clinicopathological parameters in test (G) and entire (J) cohorts. The univariate Cox regression analyses in the test (H) and entire (K) cohorts. The multivariate Cox regression analyses in the test (I) and entire (L) cohorts.

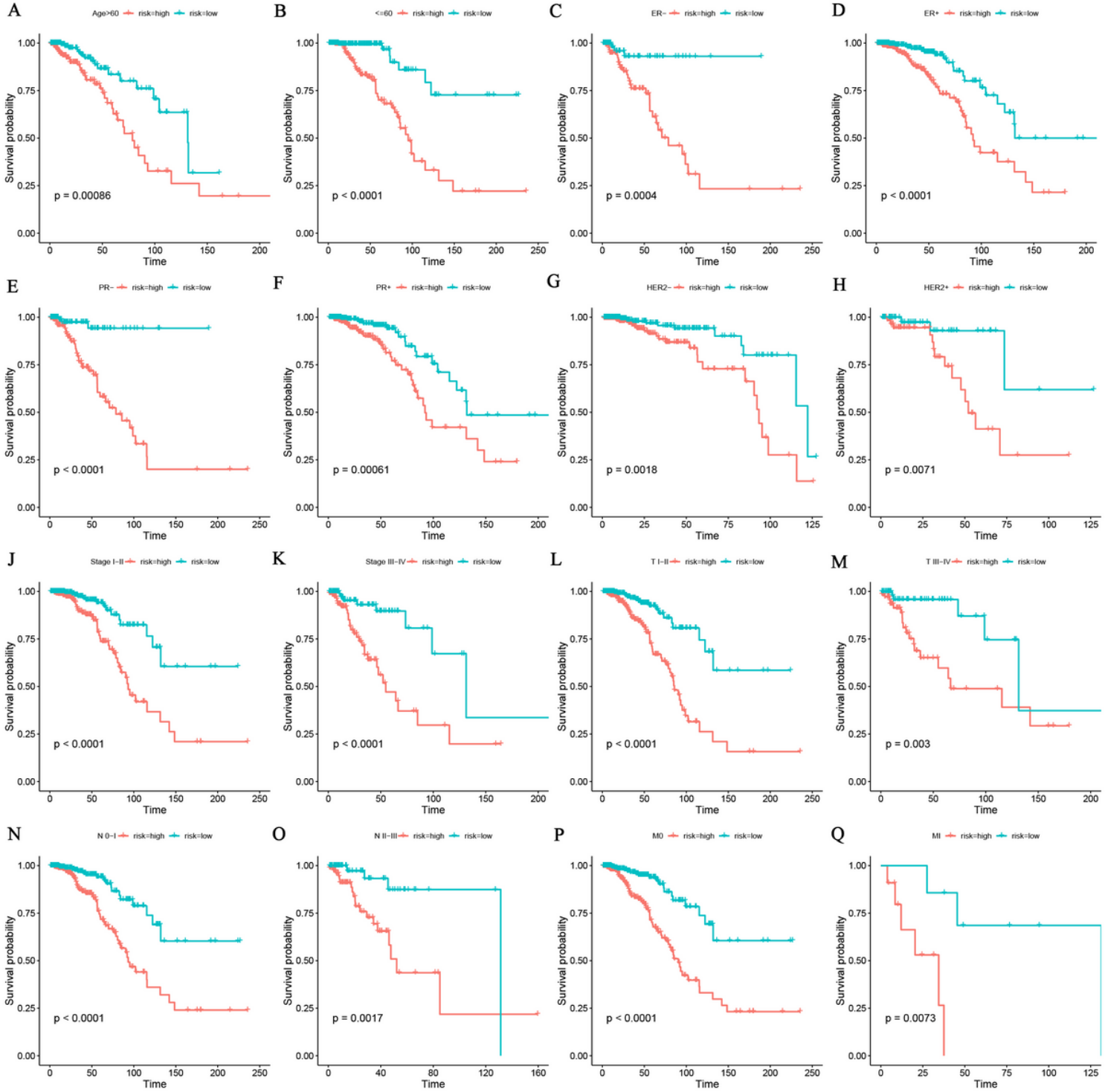

Figure 4

Stratification analyses of the prognostic signature. Kaplan-Meier curves indicated the OS of the two risk groups stratified by age (>60 years vs. ≤60 years) (A, B), ER stage (negative vs. positive) (C, D), HER2

stage (negative vs. positive) (E, F), PR stage (negative vs. positive) (G, H), stages (stage I–II vs. stage III-IV) (I, J), AJCC T stage (T I–II vs. T III-IV) (K, L), AJCC N stage (N 0-I vs. T II-III) (M, N), AJCC M stage (M 0 vs. M I) (O, P), respectively.

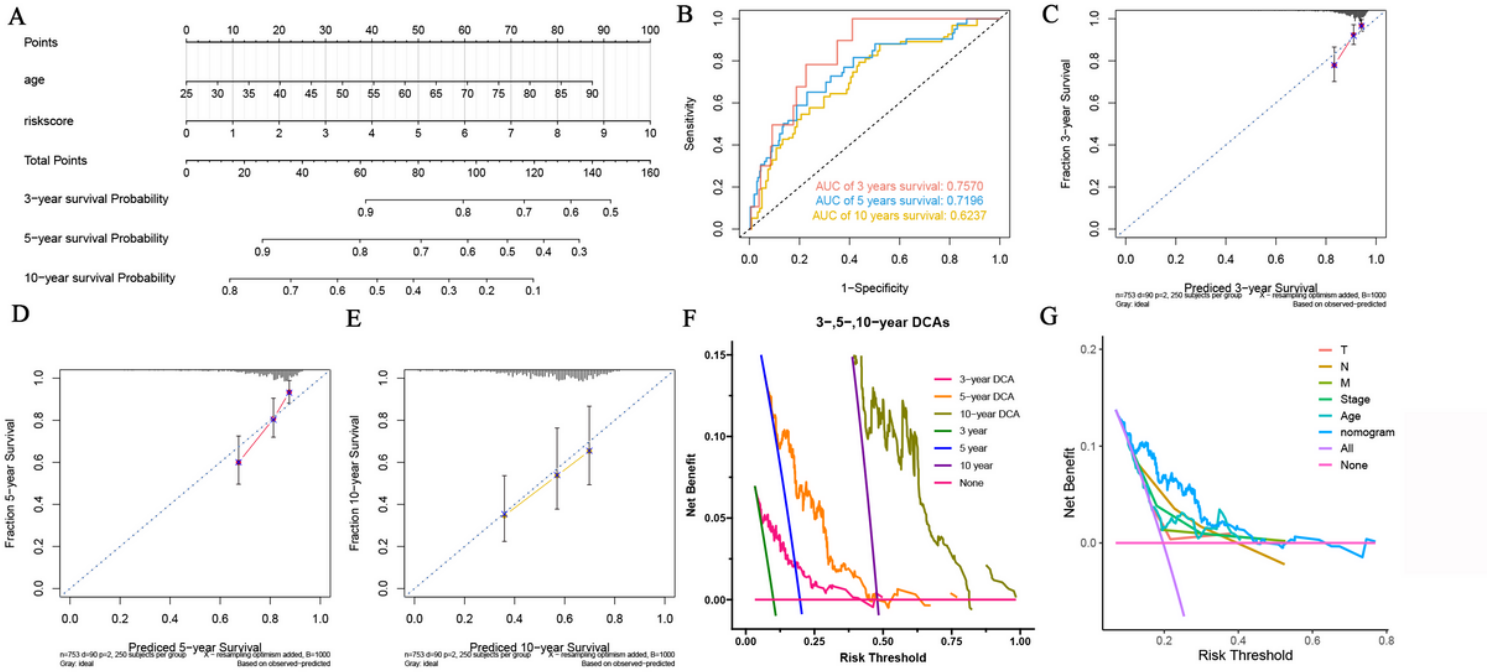

Figure 5

Construction and evaluation of the nomogram. (A) The nomogram for predicting BC patients' survival probability. (B) The nomogram's 3-, 5-, and 10-year ROC curves. (C, D, E) The 3-, 5-, and 10-year calibration curves. (F) The 3-, 5- and 10-year DCA curves of the nomogram. (G) DCA curves of clinicopathological factors and the nomogram.

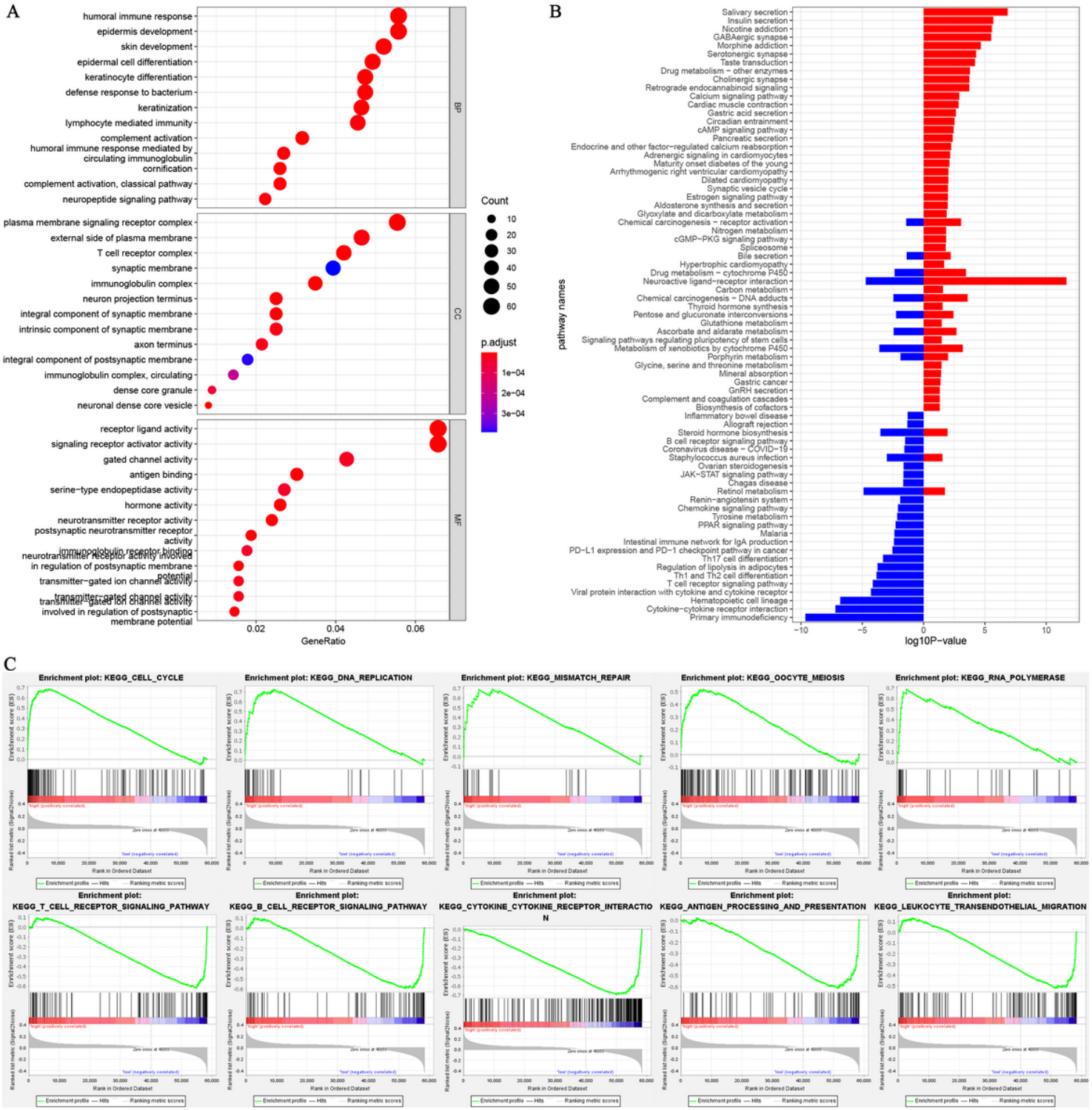

Figure 6

(A) GO enrichment analysis. (B) KEGG enrichment analysis. (C-J) The results of GSEA in two risk groups.

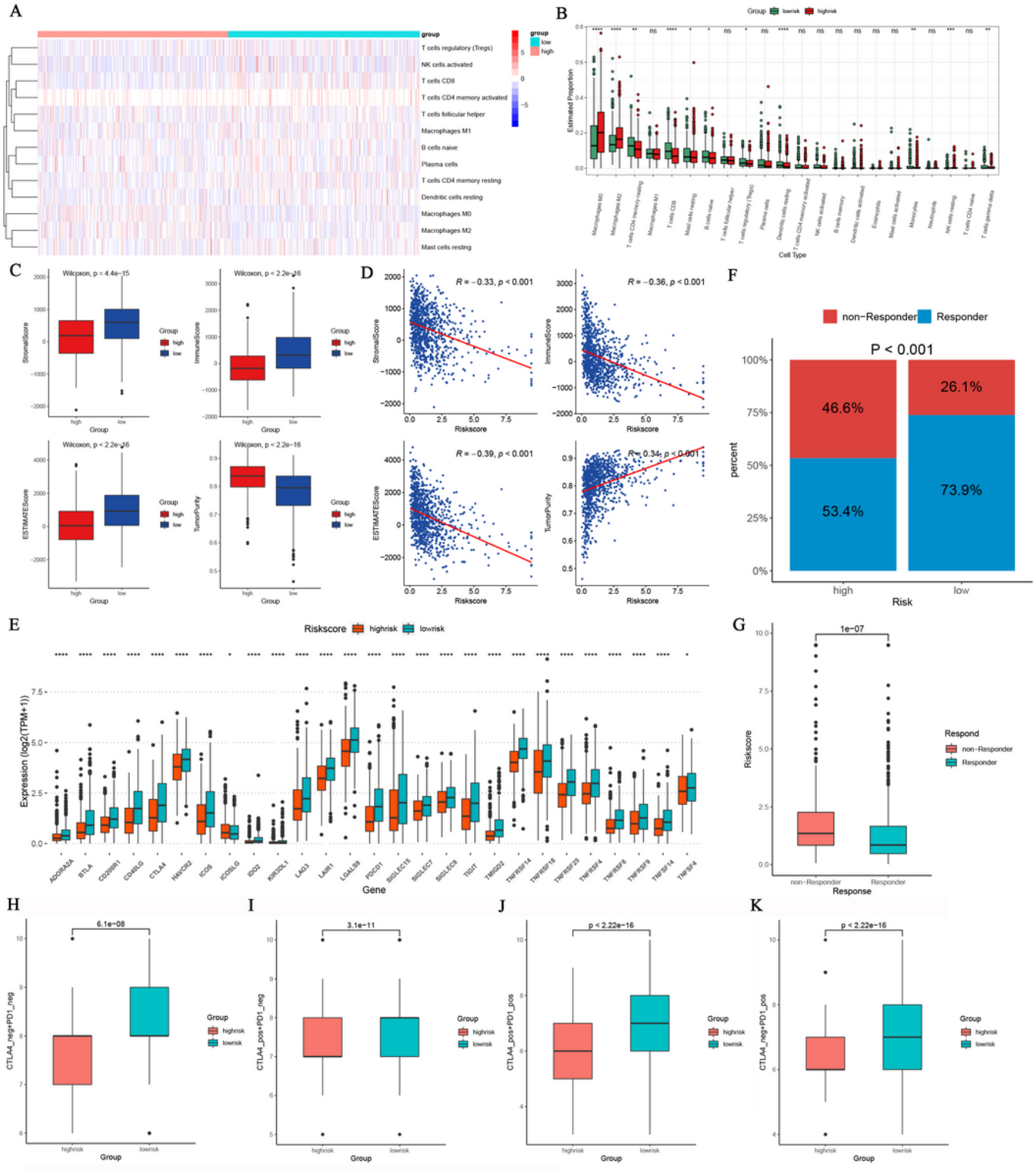

Figure 7

The immune infiltration and immunotherapy response in the two groups. (A, B) The heatmap and box plots of the proportions of tumor-infiltrating cells in the two risk groups. (C) Comparisons of tumor purity stromal, immune, and ESTIMATE scores between the two risk groups. (D) Correlations between the risk score and tumor purity, stromal, immune, and estimate score. (E) Comparisons of the 27 ICPs in the two risk groups. (F) Comparisons of the proportions of non-responders and responders to ICIs between the

two risk groups. (G) Comparison of the risk score between the responders and non-responders. (H–K) Comparison of the IPS between the two risk groups.

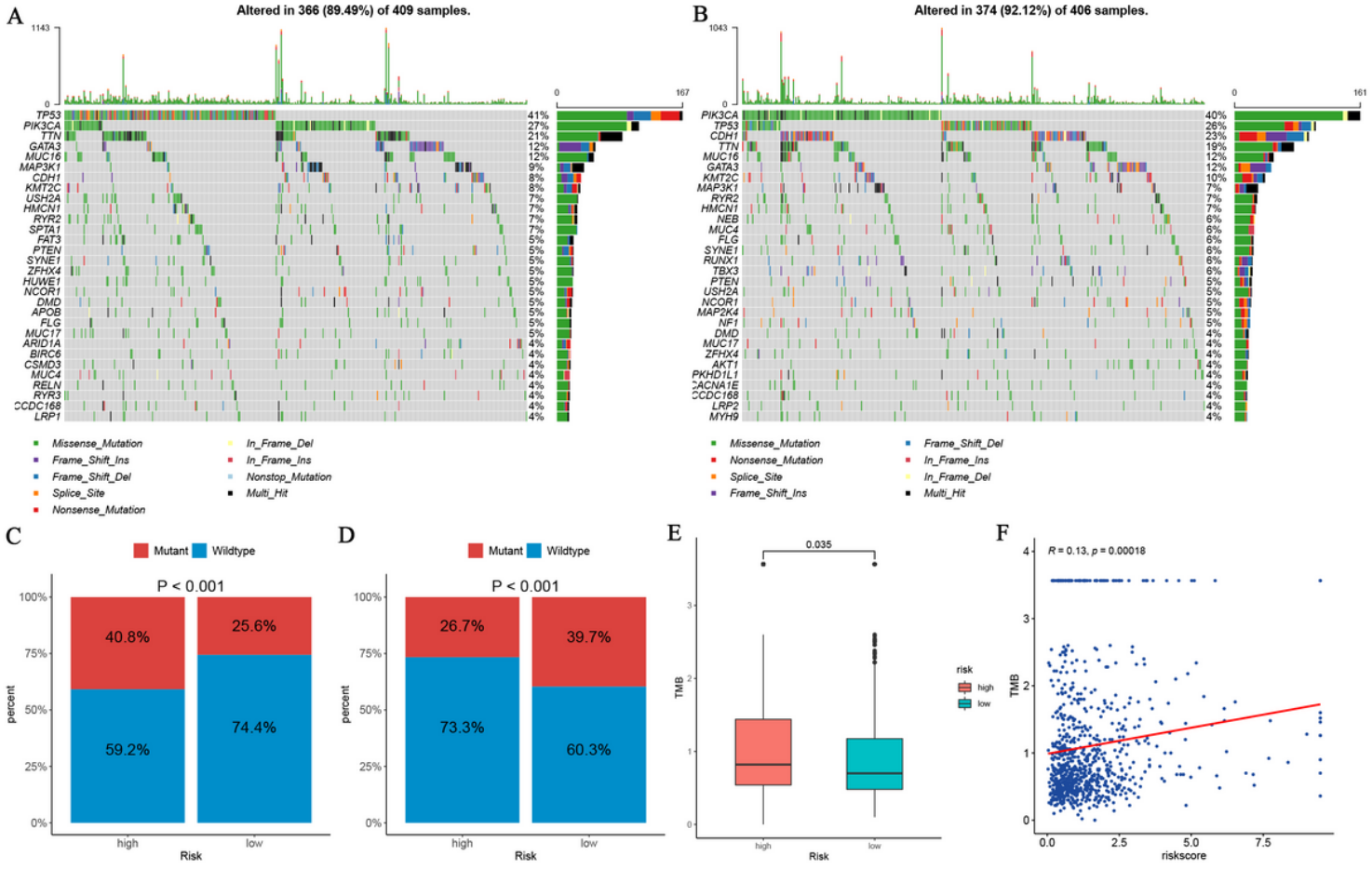

Figure 8

Association between DNA mutation and prognostic model. Waterfall plots of the top 30 mutated genes in the high-risk (A) and low-risk (B) groups. Comparisons of the mutation status of TP53 (C) and PIK3CA (D). (E) Comparisons of the TMB between the two risk groups. (F) Correlation between TMB and the risk score.

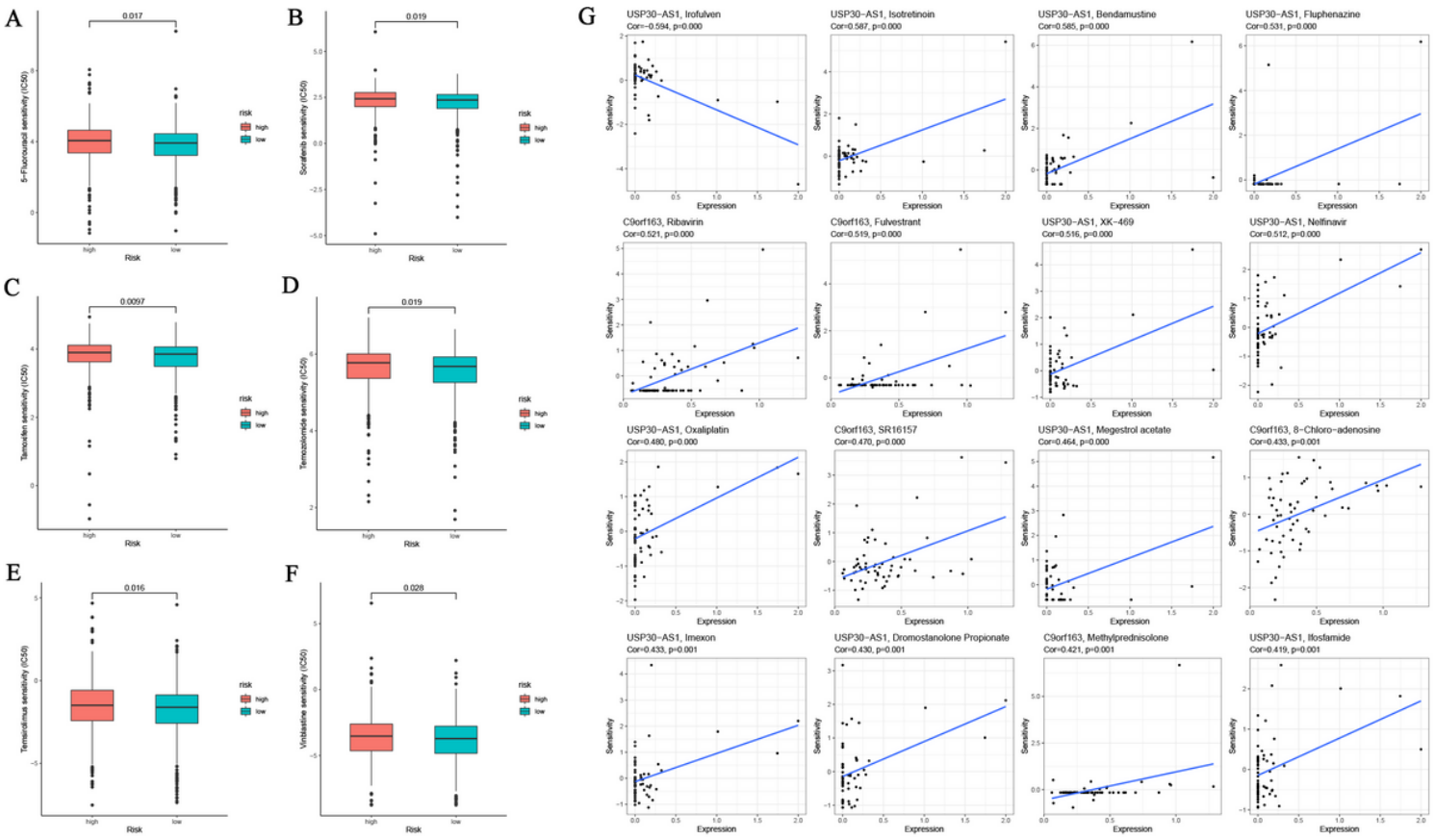

Figure 9

The sensitivity of chemotherapeutic agents and the prediction of potential drugs. The IC50 values of six chemotherapy and targeted agents in the two risk groups, including 5-Fluorouracil (A), Sorafenib (B), Tamoxifen (C), Temozolomide (D), Temsirolimus (E), and Vinblastine (F). (G) Sensitivity correlation analyses of the LRLs and potential drugs according to the CellMiner Database.

Supplementary Files

This is a list of supplementary files associated with this preprint. Click to download.

- Additionalfile1.docx